

Space- and time-like electromagnetic form factors of the nucleon

R. Bijker*

*Instituto de Ciencias Nucleares, Universidad Nacional Autónoma de México,
Apartado Postal 70-543, 04510 México, D.F., México*

Recibido el 27 de enero de 2005; aceptado el 12 de marzo de 2005

Recent experimental data on space- and time-like form factors of the nucleon are analyzed in terms of a two-component model with a quark-like intrinsic structure and a meson cloud. A good overall agreement is found for all electromagnetic form factors with the exception of the neutron magnetic form factor in the time-like region.

Keywords: Electromagnetic form factors; protons and neutrons.

Se presenta el análisis de datos experimentales recientes de los factores de forma de espacio y tiempo del nucleón. Este análisis se realiza en términos de un modelo de dos componentes con una estructura intrínseca tipo quark y una nube mesónica. Se obtuvo un buen acuerdo general para todos los factores de forma electromagnéticos con excepción del factor de forma magnético del neutrón en la región temporal.

Descriptores: Factores de forma electromagnéticos; protones y neutrones.

PACS: 13.40.Gp; 14.20.Dh

1. Introduction

The structure of the nucleon is of fundamental importance in nuclear and particle physics. The electromagnetic form factors are key ingredients to the understanding of the internal structure of composite particles like the nucleon since they contain the information about the distributions of charge and magnetization. The first evidence that the nucleon is not a point particle but has an internal structure came from the measurement of the anomalous magnetic moment of the proton in the 1930's [1], which was determined to be 2.5 times as large as one would expect for a spin 1/2 Dirac particle (the actual value is 2.793). The finite size of the proton was measured in the 1950's in electron scattering experiments at SLAC to be ~ 0.8 fm [2] (compared to the current value of 0.895 fm). The first evidence for point-like constituents (quarks) inside the proton was found in deep-inelastic-scattering experiments in the late 1960's by the MIT-SLAC collaboration [3], which eventually together with many other developments would lead to the formulation of QCD in the 1970's as the theory of strongly interacting particles.

The complex structure of the proton manifested itself once again in recent polarization transfer experiments [4, 5] which showed that the ratio of electric and magnetic form factors of the proton exhibits a dramatically different behavior as a function of the momentum transfer as compared to the generally accepted picture of form factor scaling obtained from the Rosenbluth separation method [6,7]. The discrepancy between the experimental results has been the subject of many theoretical investigations which have focussed on radiative corrections due to two-photon exchange processes [8,9].

The new experimental data for the proton form factor ratio are in excellent agreement with a phenomenological model of the nucleon put forward in 1973 [10] wherein the

external photon couples both to an intrinsic structure and to a meson cloud through the intermediate vector mesons (ρ , ω , and φ). The linear drop in the proton form factor ratio was also predicted in a chiral soliton model [11] before the polarization transfer data from Jefferson Lab became available in 2000 [4, 5]. On the contrary, the new experimental data for the neutron [12] are in agreement with the vector meson dominance (VMD) model of [10] for small values of Q^2 , but not so for higher values of Q^2 .

The aim of this contribution is to present an simultaneous study of all electromagnetic form factors of the nucleon not only in the space-like region where they can be measured in electron scattering experiments, but also in the time-like region where they can be studied through the creation or annihilation of a nucleon-antinucleon pair. The analysis is carried out in a modified version of [10]: a two-component model consisting of an intrinsic (three-quark) structure and a meson cloud whose effects are taken into account via vector meson dominance (VMD) couplings [13].

This manuscript is organized as follows: in Sec. 2 the experimental situation for the form factor ratio of the proton is reviewed briefly. The main ingredients of the two-component model of [13] and its application to the space-like form factors are discussed in Sec. 3 and extended to the time-like region in Sec. 4. The last section contains the summary and conclusions.

2. Electromagnetic form factors

Electromagnetic form factors provide important information on the structure of the nucleon. Relativistic invariance determines the form of the nucleon current for one-photon exchange to be

$$J_\mu = F_1(Q^2) \gamma^\mu + \frac{1}{2M} F_2(Q^2) i\sigma^{\mu\nu} q_\nu, \quad (1)$$

where M denotes the nucleon mass, $q = (\omega, \vec{q})$ is the four-momentum of the virtual photon and $Q^2 = -q^2$. F_1 denotes the Dirac form factor, and F_2 represents the helicity flip Pauli form factor which is proportional to the anomalous magnetic moment. The Sachs form factors, G_E and G_M , can be obtained from F_1 and F_2 by the relations

$$\begin{aligned} G_E(Q^2) &= F_1(Q^2) - \tau F_2(Q^2), \\ G_M(Q^2) &= F_1(Q^2) + F_2(Q^2), \end{aligned} \quad (2)$$

with $\tau = Q^2/4M^2$. G_E and G_M are the form factors describing the distribution of electric charge and magnetization as a function of the Q^2 satisfying

$$\begin{aligned} G_{E_{p/n}}(0) &= e_{p/n}, \\ G_{M_{p/n}}(0) &= \mu_{p/n}, \end{aligned} \quad (3)$$

where $e_{p/n}$ and $\mu_{p/n}$ denote the electric charge and magnetic moment of the proton/neutron.

2.1. Rosenbluth separation method

The differential cross section for elastic electron-nucleon scattering is given by the Rosenbluth formula [14]

$$\begin{aligned} \frac{d\sigma}{d\Omega} &= \left(\frac{d\sigma}{d\Omega} \right)_{\text{Mott}} \left[\frac{G_E^2 + \tau G_M^2}{1 + \tau} + 2\tau G_M^2 \tan^2 \frac{\theta}{2} \right] \\ &= \left(\frac{d\sigma}{d\Omega} \right)_{\text{Mott}} \frac{\tau}{\epsilon(1 + \tau)} \left[G_M^2 + \frac{\epsilon}{\tau} G_E^2 \right], \end{aligned} \quad (4)$$

where $\epsilon = 1/[1 + 2(1 + \tau) \tan^2(\theta/2)]$ is the linear polarization of the virtual photon and θ the scattering angle. For a point-like proton ($G_E = G_M = 1$) this expression reduces to the differential cross section for electron scattering off a spin-1/2 Dirac particle. By measuring the differential cross section at a fixed value of Q^2 as a function of ϵ (or equivalently, as a function of the scattering angle θ), the electric and magnetic form factors can be disentangled according to the Rosenbluth separation method. However, for large values of Q^2 the measured cross section is dominated by the magnetic form factor, which makes the determination of the electric form factor difficult due to an increasing systematic uncertainty with Q^2 . The electric and magnetic form factors obtained with the Rosenbluth method can be described to a reasonable approximation (up to the 10-20% level) by the so-called dipole fit [15]

$$\begin{aligned} G_{E_p}(Q^2) &\approx \frac{G_{M_p}(Q^2)}{\mu_p} \approx \frac{G_{M_n}(Q^2)}{\mu_n} \approx G_D(Q^2) \\ &= \frac{1}{(1 + Q^2/0.71)^2}. \end{aligned} \quad (5)$$

The electric form factor of the neutron is relatively small and was parametrized in 1971 by the the Galster formula

$$G_{E_n}(Q^2) = -\mu_n \frac{a\tau}{1 + b\tau} G_D(Q^2), \quad (6)$$

with $a=1$ and $b=5.6$ [16]. In a more recent fit, the coefficients a and b were determined to be $a = 0.888 \pm 0.023$ and $b=3.21 \pm 0.33$ [12].

2.2. Polarization transfer method

In recent years, experiments with polarized electron beams have become feasible at MIT-Bates, MAMI and Jefferson Lab. In polarization transfer experiments

$$\vec{e} + p \rightarrow e + \vec{p}, \quad (7)$$

the polarization of the recoiling proton is measured from which the ratio of the electric and magnetic form factors can be determined directly as

$$\frac{G_E}{G_M} = -\frac{P_t E + E'}{P_l 2M_p} \tan \frac{\theta}{2}, \quad (8)$$

where P_t and P_l denote the polarization of the proton perpendicular and parallel to its momentum in the scattering plane. E and E' denote the initial and final electron energy. The simultaneous measurement of the two polarization components greatly reduces the systematic uncertainties. The results of the polarization transfer method showed a big surprise. The ratio of electric and magnetic form factors of the proton dropped almost linearly with Q^2 [4,5]

$$R_p = \frac{\mu_p G_{E_p}(Q^2)}{G_{M_p}(Q^2)} \approx 1 - 0.13(Q^2 - 0.29), \quad (9)$$

in clear disagreement with the Rosenbluth results of Eq. (5) which correspond to a constant value of R_p

$$R_p \approx 1. \quad (10)$$

The vector meson dominance (VMD) model proposed in 1973 by Iachello, Jackson and Lande [10] is in excellent agreement with the new polarization transfer data, although for G_{E_p} this model is in poor agreement with the SLAC data over the entire Q^2 range [7]. Also Holzwarth predicted a linear drop in the proton form factor ratio [11] before the polarization transfer data from Jefferson Lab became available in 2000 [4,5]. Since then several theoretical calculations have reproduced this behavior [17].

To illustrate the difference between the two methods, I show in Fig. 1 the proton form factor ratio R_p obtained from the Rosenbluth separation technique [6] and from the polarization transfer experiments [4, 5]. In view of the observed discrepancy the old Rosenbluth data have been reanalyzed [18] and were found to be in agreement with form factor scaling of Eq. (10). In addition, new Rosenbluth experiments have been carried out recently at JLab [19, 20] to try to settle the contradictory experimental results. Also in this case, the new results agree within error bars with those obtained earlier at SLAC [6]. Theoretically, radiative corrections due to two-photon exchange processes are being investigated as a possible source of the observed differences [8, 9]. The importance of two-photon exchange processes can be tested experimentally by measuring the ratio of elastic electron and positron scattering off a proton [21].

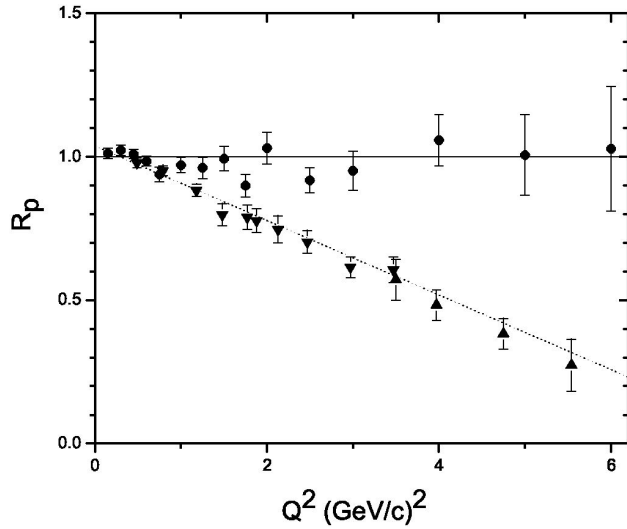


FIGURE 1. Comparison of the proton form factor ratio $R_p = \mu_p G_{E_p} / G_{M_p}$ obtained from the Rosenbluth separation method [6] (filled circles) and from the polarization transfer method [4] (filled inverted triangles) and [5] (filled triangles). The dotted and solid lines are calculated with Eqs. (9) and (10), respectively.

3. Vector meson dominance

The first models to describe the electromagnetic form factors of the nucleon are based on vector meson dominance in which it is assumed that the photon couples to the nucleon through intermediary vector mesons with the same quantum numbers as the photon [10, 22–24]. In order to take into account the coupling to the vector mesons the proton and neutron electromagnetic form factors are expressed in terms of the isoscalar, F^S , and isovector, F^V , form factors as

$$\begin{aligned} G_{M_p} &= (F_1^S + F_1^V) + (F_2^S + F_2^V), \\ G_{E_p} &= (F_1^S + F_1^V) - \tau (F_2^S + F_2^V), \\ G_{M_n} &= (F_1^S - F_1^V) + (F_2^S - F_2^V), \\ G_{E_n} &= (F_1^S - F_1^V) - \tau (F_2^S - F_2^V). \end{aligned} \quad (11)$$

In the VMD calculation of 1973 [10], the Dirac form factor was attributed to both the intrinsic structure and the meson cloud, and the Pauli form factor entirely to the meson cloud. Since this model was formulated previous to the development of QCD, no explicit reference was made to the nature of the intrinsic structure. In this contribution, the intrinsic structure is identified with a three valence quark structure. In particular, the question of whether or not there is a coupling to the intrinsic structure also in the Pauli form factor F_2 is studied. Relativistic constituent quark models in the light-front approach [25, 26] point to the occurrence of such a coupling. Dimensional counting rules [27] and the development of perturbative QCD (p-QCD) [28] has put some constraints to the asymptotic behavior of the form factors, namely that the non-spin-flip form factor $F_1 \rightarrow 1/Q^4$ and the spin-flip form factor $F_2 \rightarrow 1/Q^6$. This behavior has been very recently confirmed in a perturbative QCD re-analysis [30, 31]. The 1973

parametrization, even if it was introduced before the development of p-QCD, had this behavior. In modifying it, we insist on maintaining the asymptotic behavior of p-QCD and introduce in F_2^V a term of the type $g(Q^2)/(1 + \gamma Q^2)$. These considerations lead to the following form of the isoscalar and isovector Dirac and Pauli form factors [13]

$$\begin{aligned} F_1^S(Q^2) &= \frac{1}{2}g(Q^2) \\ &\times \left[1 - \beta_\omega - \beta_\varphi + \beta_\omega \frac{m_\omega^2}{m_\omega^2 + Q^2} + \beta_\varphi \frac{m_\varphi^2}{m_\varphi^2 + Q^2} \right], \\ F_1^V(Q^2) &= \frac{1}{2}g(Q^2) \left[1 - \beta_\rho + \beta_\rho \frac{m_\rho^2}{m_\rho^2 + Q^2} \right], \\ F_2^S(Q^2) &= \frac{1}{2}g(Q^2) \\ &\times \left[(\mu_p + \mu_n - 1 - \alpha_\varphi) \frac{m_\omega^2}{m_\omega^2 + Q^2} + \alpha_\varphi \frac{m_\varphi^2}{m_\varphi^2 + Q^2} \right], \\ F_2^V(Q^2) &= \frac{1}{2}g(Q^2) \\ &\times \left[\frac{(\mu_p - \mu_n - 1 - \alpha_\rho)}{1 + \gamma Q^2} + \alpha_\rho \frac{m_\rho^2}{m_\rho^2 + Q^2} \right], \end{aligned} \quad (12)$$

with $\mu_p = 2.793\mu_N$ and $\mu_n = -1.913\mu_N$. This parametrization insures that the three-quark contribution to the anomalous moment is purely isovector, as given by $SU(6)$. For the intrinsic form factor a dipole form $g(Q^2) = (1 + \gamma Q^2)^{-2}$ is used which is consistent with p-QCD and in addition coincides with the form used in an algebraic treatment of the intrinsic three quark structure [32]. The values of the meson masses are the standard ones: $m_\rho = 0.776$ GeV, $m_\omega = 0.783$ GeV, $m_\varphi = 1.019$ GeV.

The large width of the ρ meson is crucial for the small Q^2 behavior of the form factors and is taken into account in the same way as in [10] by the replacement [33]

$$\begin{aligned} \frac{m_\rho^2}{m_\rho^2 + Q^2} \\ \rightarrow \frac{m_\rho^2 + 8\Gamma_\rho m_\pi / \pi}{m_\rho^2 + Q^2 + (4m_\pi^2 + Q^2) \Gamma_\rho \alpha(Q^2) / m_\pi}, \end{aligned} \quad (13)$$

with

$$\alpha(Q^2) = \frac{2}{\pi} \sqrt{\frac{4m_\pi^2 + Q^2}{Q^2}} \ln \left(\frac{\sqrt{4m_\pi^2 + Q^2} + \sqrt{Q^2}}{2m_\pi} \right). \quad (14)$$

For the effective width the same value is taken as in [10, 34]: $\Gamma_\rho = 0.112$ GeV. For small values of Q^2 the form factors are dominated by the meson dynamics, whereas for large values the modification from dimensional counting laws from perturbative QCD can be taken into account by scaling Q^2 with

the strong coupling constant [23]

$$Q^2 \rightarrow Q^2 \frac{\alpha_s(0)}{\alpha_s(Q^2)} = Q^2 \frac{\ln [(\Lambda^2 + Q^2) / \Lambda_{\text{QCD}}^2]}{\ln [\Lambda^2 / \Lambda_{\text{QCD}}^2]}. \quad (15)$$

Since this modification is not very important for range of Q^2 values $0 < Q^2 < 10 \text{ GeV}^2$ considered in the present contribution, it will be neglected in the remainder.

The five remaining coefficients, β_ρ , β_ω , β_φ , α_ρ , α_φ and the parameter γ are fitted to recent data on electromagnetic form factors. Because of the inconsistencies between different data sets, most notably between those obtained from recoil polarization and Rosenbluth separation, the choice of the data plays an important role in the final outcome. In the present calculation the recoil polarization JLab data for the form factor ratios $R_p = \mu_p G_{E_p} / G_{M_p}$ and $R_n = \mu_n G_{E_n} / G_{M_n}$ are used in combination with Rosenbluth separation data, mostly from SLAC, for $G_{M_p} / \mu_p G_D$ and $G_{M_n} / \mu_n G_D$, as well as some recent measurements of G_{E_n} . The data actually used in the fit are quoted in the figure captions to Figs. 2 to 6 and are indicated by filled symbols. The values of the fitted parameters are: $\beta_\rho = 0.512$, $\beta_\omega = 1.129$, $\beta_\varphi = -0.263$, $\alpha_\rho = 2.675$, $\alpha_\varphi = -0.200$ and $\gamma = 0.515 (\text{GeV}/c)^{-2}$ [13]. These values differ somewhat from those obtained in the 1973 fit, although they retain most of their properties, namely a large coupling to the ω meson in F_1 and a very large coupling to the ρ meson in F_2 . The spatial extent of the intrinsic structure is somewhat larger than in [10], $\langle r^2 \rangle^{1/2} \simeq 0.49 \text{ fm}$ compared to $\simeq 0.34 \text{ fm}$.

Figs. 2 and 3 show a comparison between the calculation with the parameters given above and the experimental data for the proton magnetic form factor $G_{M_p} / \mu_p G_D$ and the

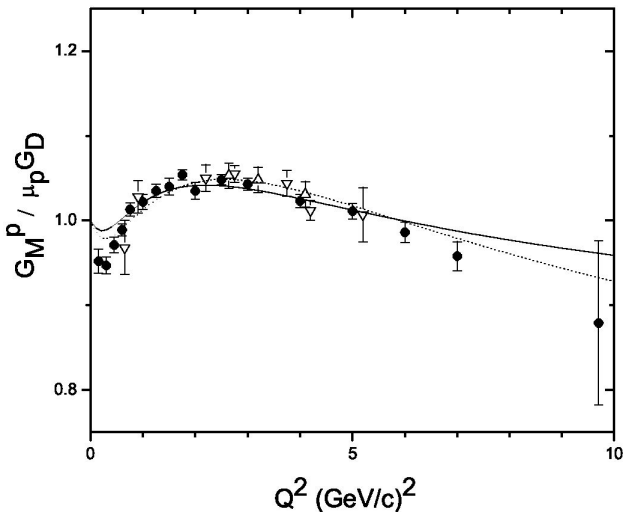


FIGURE 2. Comparison between the experimental and theoretical proton magnetic form factor $G_{M_p} / \mu_p G_D$ in the space-like region. The experimental data included in the fit are taken from [6] (filled circles). Additional data, not included in the fit, are taken from [19] (open inverted triangles) and from [20] (open triangles). The solid line is from the present calculation and the dotted line from [10].

proton form factor ratio R_p . The results of the 1973 calculation, with no direct coupling to F_2^V , are also shown. One can see that the inclusion of the direct coupling pushes the zero in R_p to larger values of Q^2 (in [34] the zero is at $\simeq 8 (\text{GeV}/c)^2$). Note that any model parametrized in terms of F_1 and F_2 will produce results for R_p that are in qualitative agreement with the data, such as a soliton model [11] or relativistic constituent quark models [25, 37]. Perturbation expansions of relativistic effects also produce results that go in the right direction [38].

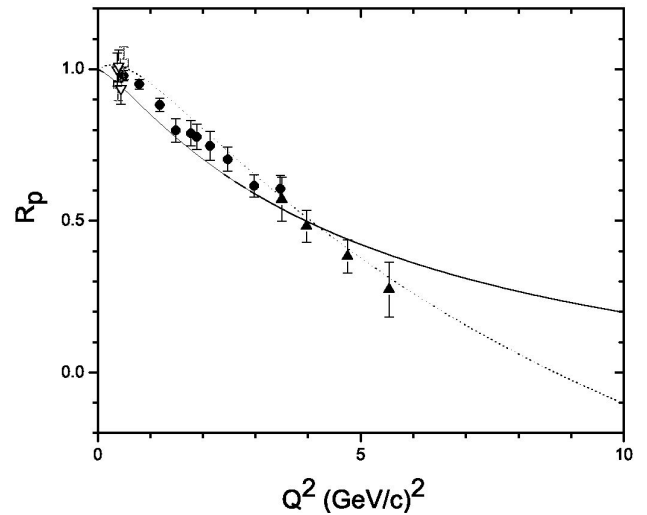


FIGURE 3. As Fig. 2, but for the proton form factor ratio $R_p = \mu_p G_{E_p} / G_{M_p}$. The experimental data included in the fit are taken from [4] (filled circles) and [5] (filled triangles). Additional data, not included in the fit, are taken from [35] (open squares) and [36] (open inverted triangles).

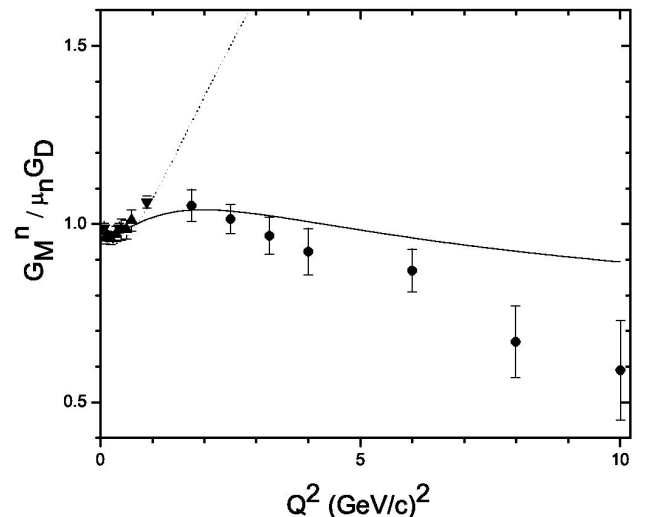


FIGURE 4. As Fig. 2, but for the neutron magnetic form factor $G_{M_n} / \mu_n G_D$. The experimental data included in the fit are taken from [39]: Rock & Lung (filled circles) and Xu (filled triangles) and [40] (filled inverted triangles).

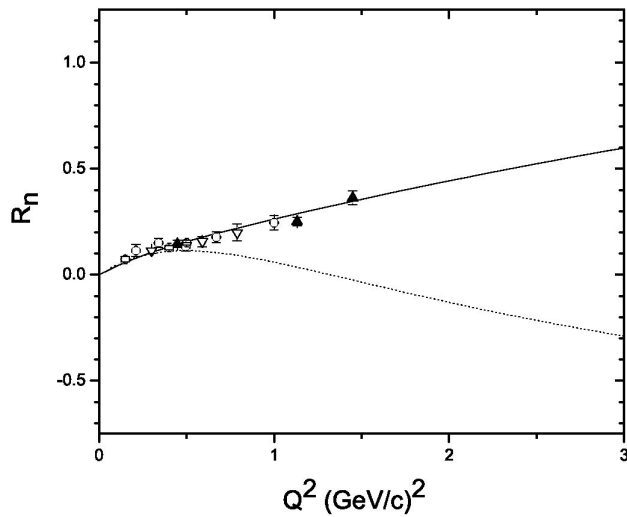


FIGURE 5. As Fig. 2, but for the neutron form factor ratio $R_n = \mu_n G_{E_n}/G_{M_n}$. The experimental data included in the fit are taken from [12] (filled triangles). Additional data, not included in the fit, are taken from [46] (open circles) and [41] (open inverted triangles).

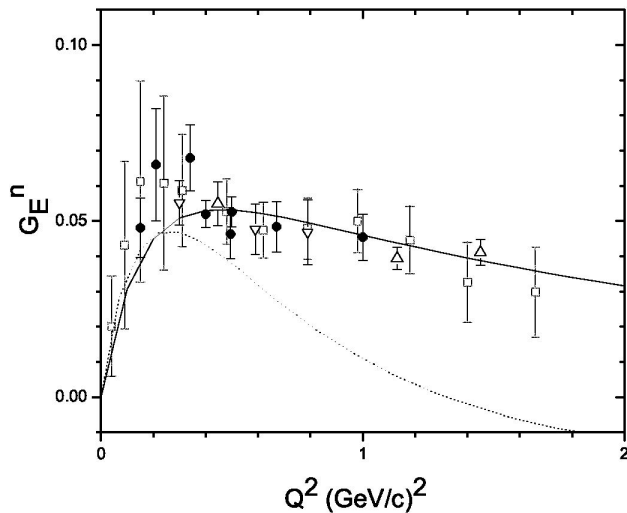


FIGURE 6. As Fig. 2, but for the neutron electric form factor G_{E_n} . The experimental data included in the fit are taken from [46] (filled circles). Additional data, not included in the fit, are taken from [12] (open triangles) [41] (open inverted triangles) and [47] (open squares).

Figs. 2 and 3 show the same comparison, but for the neutron. Contrary to the case of the 1973 parametrization, the present parametrization is in excellent agreement with the neutron data. This is emphasized in Fig. 6 where the electric form factor of the neutron is shown and compared with additional data not included in the fit. However, as one can see from Figs. 2 and 3, the excellent agreement with the neutron data is at the expense of a slight disagreement with proton data. Finally, in Fig. 7 the results for the proton electric form factor is shown in comparison with the experimental data obtained from the Rosenbluth technique. To settle the question of consistency between proton and neutron space-like data, it

is very important to extend the existing experimental information to higher values of Q^2 , more specifically:

- Measure the proton form factor ratio R_p beyond 6 $(\text{GeV}/c)^2$ among other things to see whether it indeed goes through zero or not [42].
- Measure the neutron magnetic form factor G_{M_n} beyond 2 $(\text{GeV}/c)^2$. This experiment has been carried out at JLab and is being analyzed at the moment [43].
- Measure the neutron electric form factor G_{E_n} beyond 1.4 $(\text{GeV}/c)^2$. These experiments will be carried out at JLab [44] and at MIT-Bates [45].

3.1. Charge and magnetization radii

The low Q^2 behavior of the electromagnetic form factors provides information about the charge and magnetization radii which are related to the slope of the electric and magnetic form factors in the origin by

$$\begin{aligned} \langle r^2 \rangle_E &= -6 \left. \frac{dG_E(Q^2)}{dQ^2} \right|_{Q^2=0}, \\ \langle r^2 \rangle_M &= -6 \frac{1}{\mu} \left. \frac{dG_M(Q^2)}{dQ^2} \right|_{Q^2=0}. \end{aligned} \quad (16)$$

In Table I the radii from the present calculation are compared to the experimental values. The proton charge radius and the magnetic radii of the proton and the neutron are equal within the error bars. The calculated values show the same behavior. However, the absolute values are underpredicted by a few percent (note that the radii were not included in the fit).

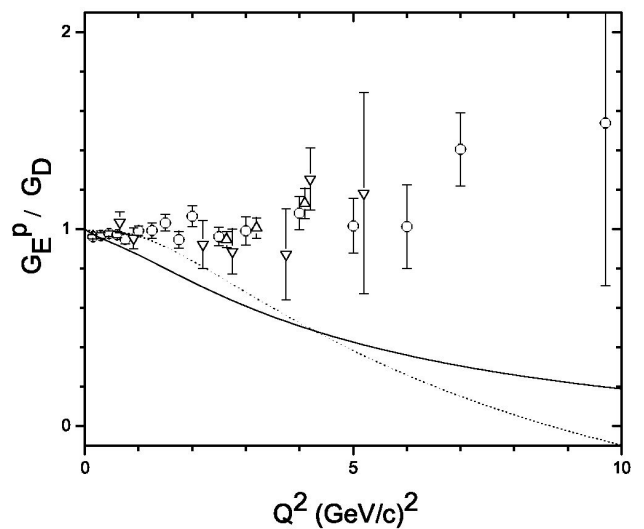


FIGURE 7. As Fig. 2, but for the proton electric form factor G_{E_p}/G_D . The experimental data, not included in the fit, are obtained from the Rosenbluth separation method [6] (open circles), [19] (open inverted triangles) and [20] (open triangles).

TABLE I. Charge and magnetization radii of the nucleon.

Radius	Present	Experiment	Reference
$\langle r^2 \rangle_{E_p}^{1/2}$	0.838	0.895 ± 0.018 fm	[48]
		0.890 ± 0.014 fm	[49]
		0.862 ± 0.012 fm	[50]
$\langle r^2 \rangle_{M_p}^{1/2}$	0.825	0.855 ± 0.035 fm	[17]
$\langle r^2 \rangle_{E_n}^{1/2}$	-0.100	-0.115 ± 0.003 fm ²	[51]
$\langle r^2 \rangle_{M_n}^{1/2}$	0.834	0.873 ± 0.011 fm	[40]

3.2. Scaling laws

Dimensional counting rules [27] and results from perturbative QCD [28] show that to leading order the ratio of Pauli and Dirac form factors scales as $F_2/F_1 \propto 1/Q^2$. However, the values extracted from the recently obtained data from polarization transfer experiments show that, at least up to $Q^2 = 5.6$ (GeV/c)², this ratio seems to scale rather as $1/Q$. In the VMD approach of [10] this $1/Q$ behavior was shown to be transient, *i.e.* it is only valid in an intermediate Q^2 region, but does not hold in the large Q^2 limit [52], whereas in a p-QCD model with nonzero quark orbital angular momenta wave it was argued that the $1/Q$ scaling may be valid to arbitrary large values of Q^2 [53]. In the latter, it was attributed to the presence of the nonzero orbital angular momentum components in the proton wave function arising from the hadron helicity nonconservation. A similar result was obtained in a relativistic constituent quark model in which the condition of Poincaré invariance induces a violation of hadron helicity conservation [54]. On the other hand, in Ref. 31 it was argued that the nonzero orbital angular momentum contributes to both F_1 and F_2 in such a way that $F_2/F_1 \propto 1/Q$ for intermediate values of Q^2 and $\propto 1/Q^2$ for large values of the momentum transfer.

In a recent p-QCD analysis of the Pauli form factor the asymptotic behavior of the ratio F_2/F_1 was predicted to be [30]

$$\frac{F_2}{F_1} \propto \frac{\ln^2(Q^2/\Lambda_{\text{QCD}}^2)}{Q^2}, \quad (17)$$

indicating that the quantity

$$A = \frac{Q^2}{\ln^2(Q^2/\Lambda_{\text{QCD}}^2)} \frac{F_2}{F_1} \propto 1, \quad (18)$$

does not depend on Q^2 in the asymptotic region. The coefficient Λ_{QCD} is a soft scale related to the size of the nucleon $\Lambda_{\text{QCD}} = 0.300$ GeV/c [17, 23]. A similar form was obtained in a study of light-front wave functions [31]. Figs. 8 and 9 show this ratio for the proton and neutron, respectively. The data seem to approach a constant value, even though the domain of validity of p-QCD is expected to set in at much higher values of Q^2 . In order to understand the onset of the

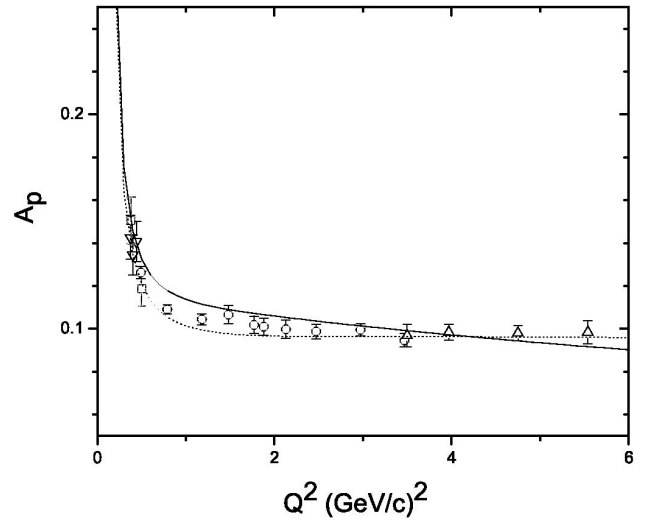


FIGURE 8. Comparison between the experimental and theoretical values of the ratio $A_p = (Q^2 F_{2,p}/F_{1,p})/\ln^2(Q^2/\Lambda_{\text{QCD}}^2)$ in the space-like region with $\Lambda_{\text{QCD}} = 0.300$ GeV/c. The experimental data are taken from [4] (open circles), [5] (open triangles), [35] (open squares) and [36] (open inverted triangles). The solid line is from the present calculation and the dotted line from [10].

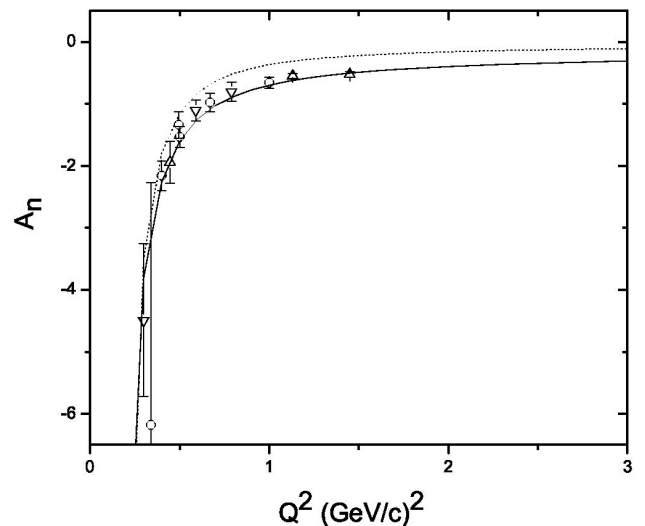


FIGURE 9. As Fig. 8, but for the neutron. The experimental data are taken from [46] (open circles), [12] (open triangles) and [41] (open inverted triangles).

perturbative region of QCD, it is crucial to extend the polarization transfer measurements to larger values of Q^2 both for the proton and the neutron.

4. Time-like form factors

Time-like form factors are important for a global understanding of the structure of the nucleon [55–59]. In the space-like region ($Q^2 > 0$) the electromagnetic form factors can be studied through electron scattering, whereas in the time-like region ($Q^2 < 0$) they can be measured through the creation

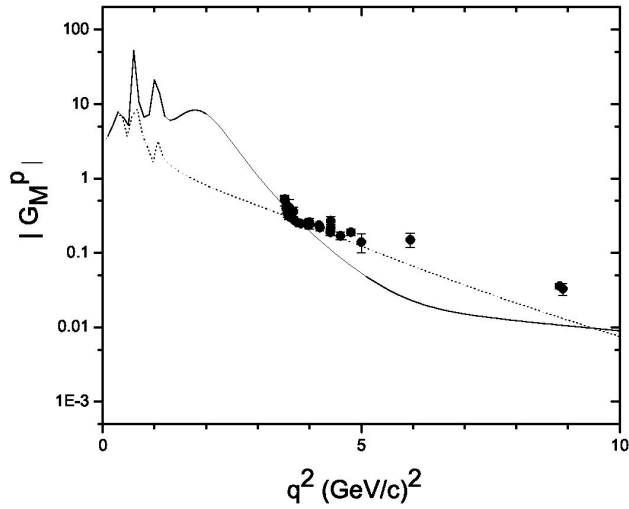


FIGURE 10. Comparison between experimental and theoretical proton magnetic form factor $|G_{M_p}|$ in the time-like region. The experimental values are taken from [60] under the assumption $|G_{E_p}| = |G_{M_p}|$. The solid lines are from the present analysis and the dotted lines from [34].

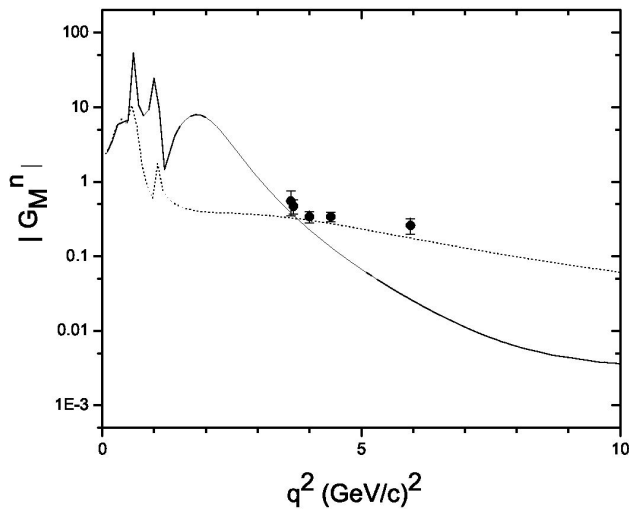


FIGURE 11. As Fig. 10, but for the neutron magnetic form factor $|G_{M_n}|$. The experimental values are taken from [61] under the assumption $|G_{E_n}| = 0$.

or annihilation of a nucleon-antinucleon pair. The time-like structure of the nucleon form factors has recently been analyzed [34] in the VMD model of [10]. Here the same approach is used to analyze the time-like structure of the form factors. The method consists in analytically continuing the intrinsic structure to [13]

$$g(q^2) = \frac{1}{(1 - \gamma e^{i\theta} q^2)^2}, \quad (19)$$

where $q^2 = -Q^2$ and θ is a phase. The contribution of the ρ meson is analytically continued for $q^2 > 4m_\pi^2$ as [33]

$$\frac{m_\rho^2}{m_\rho^2 - q^2} \rightarrow \frac{m_\rho^2 + 8\Gamma_\rho m_\pi / \pi}{m_\rho^2 - q^2 + (4m_\pi^2 - q^2)\Gamma_\rho[\alpha(q^2) - i\beta(q^2)]/m_\pi}, \quad (20)$$

where

$$\alpha(q^2) = \frac{2}{\pi} \sqrt{\frac{q^2 - 4m_\pi^2}{q^2}} \ln \left(\frac{\sqrt{q^2 - 4m_\pi^2} + \sqrt{q^2}}{2m_\pi} \right),$$

$$\beta(q^2) = \sqrt{\frac{q^2 - 4m_\pi^2}{q^2}}. \quad (21)$$

The results for the time-like form factors are shown in Figs. 10 and 11. The phase θ is obtained from a best fit to the proton data: $\theta = 0.397 \text{ rad} \simeq 22.7^\circ$, compared to the value $\simeq 53^\circ$ obtained in [34]. It should be noted that the correction to the large q^2 data discussed in [34] has not been done in these figures. One can see from these figures that while the proton form factor, $|G_{M_p}|$, obtained from analytic continuation of the present parametrization is in marginal agreement with data, the neutron form factor, $|G_{M_n}|$, is in major disagreement. This result points once more to the inconsistency between neutron space-like and time-like data already noted in Refs. 34 and 55. A remeasurement of the neutron time-like data could help to resolve this inconsistency. The result presented here is in contrast with the analysis of [34] that was in good agreement with both proton and neutron time-like form factors. In Figs. 12 and 13, the electric form factors $|G_{E_p}|$ and $|G_{E_n}|$ are shown for future use in the extraction of $|G_{M_p}|$ and $|G_{M_n}|$ from the data. These figures show that the assumptions $|G_{E_p}| = |G_{M_p}|$ and $|G_{E_n}| = 0$ used in the extraction of the magnetic form factors from the experimental data, are not always justified.

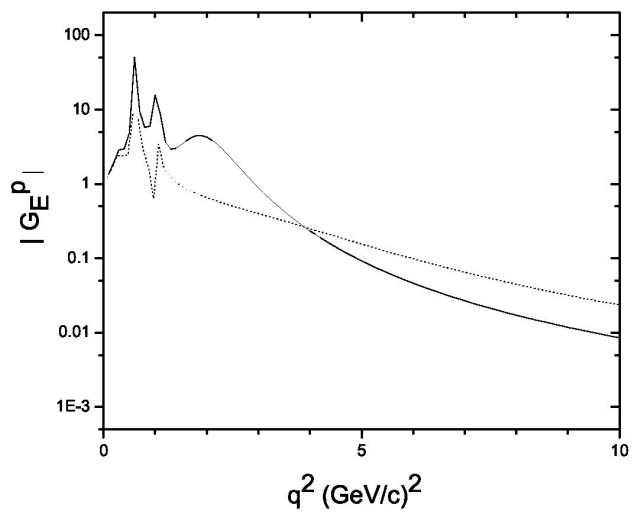


FIGURE 12. As Fig. 10, but for the proton electric form factor $|G_{E_p}|$.

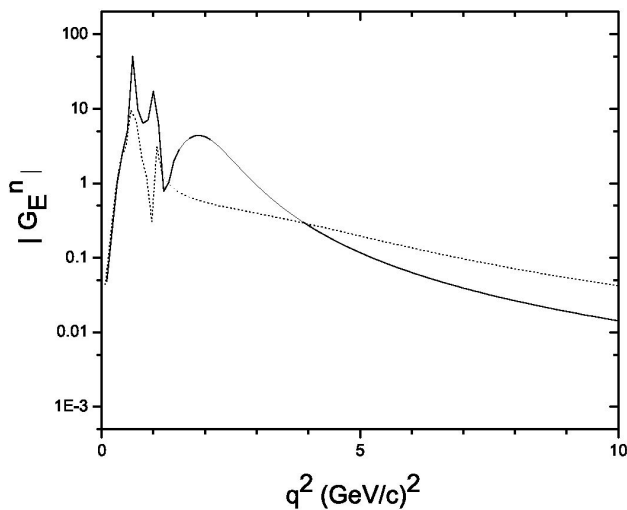


FIGURE 13. As Fig. 10, but for the neutron electric form factor $|G_{E_n}|$.

5. Summary and conclusions

In this contribution, a simultaneous study of the space- and time-like data on the electromagnetic form factors of the nucleon was presented. The analysis was carried out in a two-component model, which consists of an intrinsic (three-quark) structure and a meson cloud whose effects were taken into account via VMD couplings to the ρ , ω and φ mesons. The difference with an earlier calculation lies in the treatment of the isovector Pauli form factor F_2^V . The inclusion of an intrinsic component in F_2^V shows a considerable improvement for the space-like neutron form factors. Since the form fac-

tors are related by isospin symmetry, the excellent description of the neutron form factors is at the expense of a slight disagreement for the proton space-like data. The picture emerging from the present study is that of an intrinsic structure slightly larger in spatial extent than that of [34], $\langle r^2 \rangle^{1/2} \simeq 0.49$ fm instead of 0.34 fm, and a contribution of the meson cloud ($q\bar{q}$ pairs) slightly smaller in strength than that of [34], $\alpha_\rho = 2.675$ instead of 3.706.

The present calculation is not able to describe the neutron time-like data in a satisfactory way. In effect, a simultaneous description of both the space- and time-like data for the neutron has encountered serious difficulty in the literature [13, 34, 55]. It is of the utmost importance to extend the experimental information on the neutron form factors to be able to resolve the observed discrepancies and to obtain a consistent description of all electromagnetic form factors of the nucleon in both the space- and time-like regions.

Recently it was shown [58, 59] that the angular dependence of the single-spin and double-spin polarization observables provides a sensitive test of model of nucleon form factors in the time-like region. These polarization observables allow to distinguish between different models of nucleon electromagnetic form factors, even though they fit equally well the nucleon form factors in the space-like region. More work in this direction is in progress.

Acknowledgments

This work was supported in part by Conacyt, Mexico. It is a pleasure to thank Franco Iachello and Kees de Jager for stimulating discussions.

* Invited talk at 'XXVIII Nuclear Physics Symposium', Coconoc, México, January 4-7, 2005.

1. I. Estermann, R. Frisch, and O. Stern, *Nature* **132** (1933) 169.
2. R. Hofstadter, *Annu. Rev. Nucl. Sci.* **7** (1957) 231.
3. J.I. Friedman and H.W. Kendall, *Annu. Rev. Nucl. Sci.* **22** (1972) 203.
4. M.K. Jones *et al.*, *Phys. Rev. Lett.* **84** (2000) 1398; V. Punjabi *et al.*, nucl-ex/0501018.
5. O. Gayou *et al.*, *Phys. Rev. C* **64** (2001) 038202; O. Gayou *et al.*, *Phys. Rev. Lett.* **88** (2002) 092301.
6. R.C. Walker *et al.*, *Phys. Rev. D* **49** (1994) 5671.
7. L. Andivahis *et al.*, *Phys. Rev. D* **50** (1994) 5491.
8. P.A.M. Guichon and M. Vanderhaeghen, *Phys. Rev. Lett.* **91** (2003) 142303; P.G. Blunden, W. Melnitchouk, and J.A. Tjon, *Phys. Rev. Lett.* **91** (2003) 142304; Y.-C. Chen, A. Afanasev, S.J. Brodsky, C.E. Carlson, and M. Vanderhaeghen, *Phys. Rev. Lett.* **93** (2004) 122301; P.G. Blunden, W. Melnitchouk, and J.A. Tjon, arXiv:nucl-th/0506039.
9. M.P. Rekalo and E. Tomasi-Gustafsson, *Nucl. Phys. A* **740** (2004) 271; *Nucl. Phys. A* **742** (2004) 322; *Eur. Phys. J. A* **22** (2004) 331.
10. F. Iachello, A.D. Jackson, and A. Lande, *Phys. Lett. B* **43** (1973) 191.
11. G. Holzwarth, *Z. Phys. A* **356** (1996) 339.
12. R. Madey *et al.*, *Phys. Rev. Lett.* **91** (2003) 122002.
13. R. Bijker and F. Iachello, *Phys. Rev. C* **69** (2004) 068201.
14. M.N. Rosenbluth, *Phys. Rev.* **79** (1950) 615.
15. P. Bosted *et al.*, *Phys. Rev. C* **51** (1995) 409.
16. S. Galster, H. Klein, J. Moritz, K.H. Schmidt, and D. Wegener, *Nucl. Phys. B* **32** (1971) 221.
17. C.E. Hyde-Wright and K. de Jager, *Annu. Rev. Nucl. Part. Sci.* **54** (2004) 217 (updated version, arXiv:nucl-ex/0507001).
18. J. Arrington, *Phys. Rev. C* **68** (2003) 034325.
19. M.E. Christy *et al.*, *Phys. Rev. C* **70** (2004) 015206.
20. I.A. Qattan *et al.*, nucl-ex/0410010.
21. J. Arrington *et al.*, arXiv:nucl-ex/0408020.
22. G. Höhler *et al.*, *Nucl. Phys. B* **114** (1976) 505.

23. M.F. Gari and W. Krümpelmann, *Phys. Lett. B* **141** (1984) 295; *Z. Phys. A* **322** (1985) 689; *Phys. Lett. B* **173** (1986) 10.
24. E.L. Lomon, *Phys. Rev. C* **64** (2001) 035204.
25. M.R. Frank, B.K. Jennings, and G.A. Miller, *Phys. Rev. C* **54** (1996) 920.
26. E. Pace, G. Salmè, F. Cardarelli, and S. Simula, *Nucl. Phys. A* **666** (2000) 33c.
27. S.J. Brodsky and G.R. Farrar, *Phys. Rev. Lett.* **31** (1973) 1153; *Phys. Rev. D* **11** (1975) 1309; V.A. Matveev, R.M. Muradian, and A.N. Tavkhelidze, *Lett. Nuovo Cimento* **7** (1973) 719.
28. G.P. Lepage and S.J. Brodsky, *Phys. Rev. Lett.* **43** (1979) 545; *Phys. Rev. D* **22** (1980) 2157.
29. A. Akhiezer and M.P. Rekaló, *Dokl. Akad. Nauk USSR* **180** (1968) 1081; *Sov. J. Part. Nucl.* **4** (1974) 277.
30. A.V. Belitsky, X. Ji, and F. Yuan, *Phys. Rev. Lett.* **91** (2003) 092003.
31. S.J. Brodsky, J.R. Hiller, D.S. Hwang, and V.A. Karmanov, *Phys. Rev. D* **69** (2004) 076001.
32. R. Bijker, F. Iachello, and A. Leviatan, *Ann. Phys. (N.Y.)* **236** (1994) 69; *Phys. Rev. C* **54** (1996) 1935.
33. W.R. Frazer and J.R. Fulco, *Phys. Rev.* **117** (1960) 1609.
34. F. Iachello and Q. Wan, *Phys. Rev. C* **69** (2004) 055204.
35. B.D. Milbrath *et al.*, *Phys. Rev. Lett.* **80** (1998) 452; erratum *Phys. Rev. Lett.* **82** (1999) 2221.
36. Th. Pospischil *et al.*, *Eur. Phys. J. A* **12** (2001) 125.
37. F. Cardarelli and S. Simula, *Phys. Rev. C* **62** (2000) 065201.
38. M. De Sanctis, M.M. Giannini, L. Repetto, and E. Santopinto, *Phys. Rev. C* **62** (2000) 025208; M. De Sanctis, M.M. Giannini, E. Santopinto, and A. Vassallo, *Eur. Phys. J. A* **19** (2004) 81; *Rev. Mex. Fís.* **50 S2** (2004) 96.
39. S. Rock *et al.*, *Phys. Rev. D* **46** (1992) 24; A. Lung *et al.*, *Phys. Rev. Lett.* **70** (1993) 718; W. Xu *et al.*, *Phys. Rev. Lett.* **85** (2000) 2900; W. Xu *et al.*, *Phys. Rev. C* **67** (2003) 012201.
40. G. Kubon *et al.*, *Phys. Lett. B* **524** (2002) 26.
41. D.I. Glazier *et al.*, arXiv:nucl-ex/0410026.
42. C. Perdrisat *et al.*, JLab Experiment E01-109.
43. W.K. Brooks *et al.*, JLab Experiment E94-017; W.K. Brooks and J.D. Lachniet, arXiv:nucl-ex/0504028.
44. B. Wojtsekhowski *et al.*, JLab Experiment E02-013; R. Madey *et al.*, JLab Experiment E04-110.
45. R. Alarcon *et al.*, MIT-Bates proposal E91-09.
46. C. Herberg *et al.*, *Eur. Phys. J. A* **5** (1999) 131 applies FSI corrections to M. Ostrick *et al.*, *Phys. Rev. Lett.* **83** (1999) 276; I. Passchier *et al.*, *Phys. Rev. Lett.* **82** (1999) 4988; H. Zhu *et al.*, *Phys. Rev. Lett.* **87** (2001) 081801; J. Golak *et al.*, *Phys. Rev. C* **63** (2001) 034006 applies FSI corrections to J. Becker *et al.*, *Eur. Phys. J. A* **6** (1999) 329; J. Bermuth *et al.*, *Phys. Lett. B* **564** (2003) 199 updates D. Rohe *et al.*, *Phys. Rev. Lett.* **83** (1999) 4257; G. Warren *et al.*, *Phys. Rev. Lett.* **92** (2004) 04230.
47. R. Schiavilla and I. Sick, *Phys. Rev. C* **64** (2001) 041002.
48. I. Sick, *Phys. Lett. B* **576** (2003) 62.
49. Th. Udem *et al.*, *Phys. Rev. Lett.* **79** (1997) 2646.
50. G.G. Simon, Ch. Schmitt, F. Borkowski, and V.H. Walther, *Nucl. Phys. A* **333** (1980) 381.
51. S. Kopecky *et al.*, *Phys. Rev. C* **56** (1997) 2229.
52. F. Iachello, *Eur. Phys. J. A* **19** (2004) 29.
53. J.P. Ralston and P. Jain, *Phys. Rev. D* **69** (2004) 053008.
54. G.A. Miller and M.R. Frank, *Phys. Rev. C* **65** (2002) 065205.
55. H.-W. Hammer, U.-G. Meissner, and D. Drechsel, *Phys. Lett. B* **385** (1996) 343.
56. S. Dubničká, A.Z. Dubničková, and P. Weisenpacher, *J. Phys. G: Nucl. Part. Phys.* **29** (2003) 405.
57. E. Tomasi-Gustafsson and M.P. Rekaló, *Phys. Lett. B* **504** (2001) 291.
58. S.J. Brodsky, C.E. Carlson, J.R. Hiller, and D.S. Hwang, *Phys. Rev. D* **69** (2004) 054022.
59. E. Tomasi-Gustafsson, F. Lacroix, C. Duterte, and G.I. Gakh, *Eur. Phys. J. A* **24** (2005) 419 [arXiv:nucl-th/0503001].
60. M. Castellano *et al.*, *Il Nuovo Cimento A* **14** (1973) 1; G. Basompierre *et al.*, *Phys. Lett. B* **68** (1977) 477; D. Bisello *et al.*, *Nucl. Phys. B* **224** (1983) 379; T.A. Armstrong *et al.*, *Phys. Rev. Lett.* **70** (1993) 1212; G. Bardin *et al.*, *Nucl. Phys. B* **411** (1994) 3; A. Antonelli *et al.*, *Phys. Lett. B* **334** (1994) 431; M. Ambrogiani *et al.*, *Phys. Rev. D* **60** (1999) 032002.
61. A. Antonelli *et al.*, *Nucl. Phys. B* **517** (1998) 3.